ICSV28
SINGAPORE
24 - 28 JULY 2022
28th International Congress on Sound and Vibration
The annual congress of the International Institute of Acoustics and Vibration (IIAV)
SAS

REDUCED-ORDER AEROACOUSTIC MODELING OF ELECTRONICS COOLING FANS

Wenguang Zhao, Sahan Wasala and Tim Persoons
Dept. Mechanical, Manufacturing & Biomedical Engineering, Trinity College Dublin, Dublin, Ireland
e-mail: wzhao@tcd.ie

As the trend of compact packaging and high-density thermal management continues, the acoustic noise emission from electronics cooling fans is becoming a critical concern. High-fidelity computational fluid dynamics (CFD) combined with computational aeroacoustics (CAA) techniques are commonly regarded as viable solutions for simulating cooling fan noise. However, when used as a design and optimization approach, the high-fidelity method presents a significant hurdle in terms of computational costs. Therefore, a reduced-order yet accurate noise prediction tool would be highly desirable for industrial design teams. This study focuses on the reduced-order modeling of the aerodynamic and aeroacoustic performance of an isolated axial fan used in electronic cooling applications. A reduced-order model (ROM) was proposed based on blade element theory (BET) and the Ffowcs Williams-Hawkings (FW-H) acoustic analogy, and its accuracy was validated against available benchmark cases. The ROM's results demonstrate reasonable agreement with the experimental results while requiring a significantly low computational cost, i.e., under 1% compared to a high-fidelity CFD simulation, making it appropriate for low-noise fan design and optimization.
Keywords: aeroacoustics, reduced-order modeling, fan curves, broadband noise, tonal noise

1. Introduction

Thermal management of hard disk drive (HDD) system in data centers (DCs) relies heavily on forced air cooling. The cooling system, which consists of arrays of axial fans, may cause excessive acoustic noise disturbance in DCs, endangering human hearing and decreasing HDD operational reliability [1]. Furthermore, as the continuous development of compact packaging and high-power densities of electronic components in DCs, air movement in confined channels within compact enclosures leads to increased inflow distortions and stronger acoustic noise generation [2].

In the typical electronics cooling fans, low Reynolds number flows ranging from $Re = 10^4$–10^5 typically occur due to the small-scale blades. The flow separates easily from the blade surface in this range and does not reattach [3]. As a result, the aerodynamic phenomena and noise generation mechanisms are different from the high Reynolds number flows encountered by large aircraft rotors. The high-fidelity

large eddy simulation (LES) method is commonly utilized to calculate the aerodynamic performance at low Re flows, but it is computationally expensive and difficult to integrate into an acoustic optimization process [1, 4]. The fan acoustic performance data provided by manufacturers is typically just one overall sound pressure level value without accounting for any back pressure effects within enclosures, which is quite limited for the system level design and optimization. Hence, a quick evaluation tool for calculating the aerodynamic and acoustic performance of a fan would be extremely valuable for system assessments, as well as providing insight into future noise controls.

The present paper focuses on the developments and validations of a reduced order model (ROM) to fast evaluate the aerodynamic and aeroacoustic performance of electronics cooling fans at low Re flows. The ROM should be fast and reliable enough to be integrated into an aeroacoustic design and optimization tool. This will open the path for a fan design with less adverse acoustic emissions at low Re flows. To accomplish that, the BET-based methods are used as a flow solver. The far field broadband noise and tonal noise are derived using Amiet's model [5] and the FW-H equation [6], respectively. All the models in this ROM code are implemented in MATLAB.

2. Numerical methods

In this section, the numerical approaches used for aerodynamics and acoustics are introduced.

2.1 Aerodynamic analysis

The analytical method used in this work is based on the blade element theory (BET) combined with momentum theory (MT) or lifting-line theory (LLT). The blade element theory is also referred to as strip theory. It can be used to analyze the blade force of the fan by dividing the blade into a number of spanwise elements, which is illustrated in Fig. 1(a). The main assumption of this theory is that each spanwise element is independent, and the loading of each blade element can be determined without considering the interactions between those radial elements. The inflow schematic of a typical fan is illustrated in Fig. 1(a). Following the classical BET implementation [7], the thrust dT and torque dM for a radial element dr can be given as

$$dT = \frac{1}{2}\rho B v^2 c C_n dr = \frac{1}{2}\rho B \frac{\Omega^2 r^2 (1-a')^2}{\cos^2\phi} c C_n dr \tag{1}$$

$$dM = \frac{1}{2}\rho B v^2 c C_t r dr = \frac{1}{2}\rho B \frac{\Omega^2 r^2 (1-a')^2}{\cos^2\phi} c C_t r dr, \tag{2}$$

where C_n is the force coefficient normal to the rotor plane ($C_n = C_l \cos\phi - C_d \sin\phi$), C_t is the force coefficient tangential to the rotor plane ($\mathrm{C}_t = \mathrm{C}_l \sin\phi + \mathrm{C}_d \cos\phi$), c is the blade sectional chord, B is the number of blades, v is the total velocity at each radial element ($v = \sqrt{{u_n}^2 + {u_t}^2}$). u_n and u_t are the axial velocity and tangential velocity respectively. a' is the tangential velocity induction factor ($u_t = \Omega r\,(1-a')$) and a is the axial velocity induction factor, which normally can be expressed as a function of inflow wind velocity ($u_n = v_\infty\,(1+a)$). ϕ is the flow induction angle and $\phi = \tan^{-1} u_n/u_t$. The sectional angle of attack α, which can be calculated using the known geometrical pitch angle β, is $\alpha = \beta - \phi$. The sectional lift and drag coefficients C_l and C_d are calculated by polynomially interpolation from a pre-computed look-up table based on the angle of attack α. For the sake of numerical robustness, all the aerodynamic data of the 2D airfoil in the table were calculated by XFOIL [8] in the angle of attack range from $-20°$ to $+20°$, and then extended to the entire $\pm 180°$ angle of attack range using the Viterna method [9].

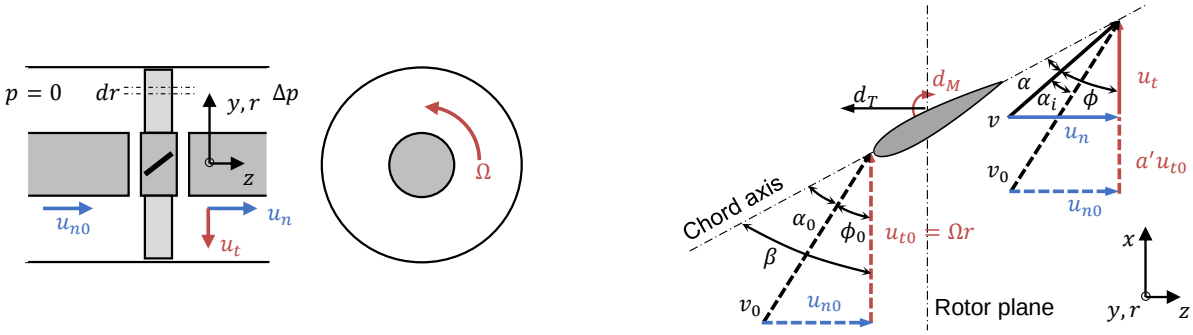

(a) Schematic of the inflow of a typical fan (b) Velocities and forces at a typical blade element

Figure 1: Definition of variables for an axial fan geometry.

It is insufficient to obtain the aerodynamic performance only with BET. The flow field is usually determined by combining it with another theory. Blade element momentum theory (BEMT), the combination of BET and one-dimensional momentum theory, is a widely used method for rotating blade calculation [7]. From the momentum balance, the thrust and torque for a circular radial element dr can also be given as

$$dT = 4\pi r \rho v_\infty^2 a(1+a)dr \tag{3}$$

$$dM = 4\pi r^3 \rho v_\infty \Omega(1+a)a'dr. \tag{4}$$

By solving Eqs. (1) to (4), the axial and tangential induction factors can be obtained iteratively. The BEMT method is well-defined and validated for open rotor applications [4]. However, the traditional BEMT method is not applicable to a shrouded or ducted rotor with back pressure effect, because the shroud alters the flow structure, making momentum equations based on stream tube assumption invalid [10].

In this work, a lifting-line theory-based method was developed for fan flow calculations assuming an elliptical lift distribution along the fan blade. The velocities and forces of one 2D airfoil at the fan inlet and outlet are illustrated in Fig. 1(b). For a fan with a cylindrical shroud, the axial velocity is constant according to the continuity equation. Assuming an elliptical lift distribution on a finite span blade with geometrical aspect ratio AR, the induced angle of attack can be readily determined as $\alpha_i = C_l/\pi AR_{eff}$ [11]. The effective aspect ratio AR_{eff} is defined in this paper based on the aspect ratio multiplying a correction factor M_{AR} ($AR_{eff} = AR \times M_{AR}$). The correction multiplier M_{AR} is utilized to take into account the effect of the shroud suppressing tip vortices, which can be interpreted as an increase in effective aspect ratio ($M_{AR} > 1$). The tangential induced velocity a', whose effect is to decrease the tangential velocity, can be expressed as

$$a' = \frac{v_0}{\Omega r} \sin\phi \tan\left(\frac{C_l}{\pi AR_{eff}}\right), \tag{5}$$

where v_0 is the total velocity at the fan inlet ($v_0 = \sqrt{{u_{n0}}^2 + {u_{t0}}^2}$), u_{n0} can be obtained by the total flow rate Q and the flow area A ($u_{n0} = Q/A$). The lift coefficients for 3D finite blades are corrected based on the C_l results of 2D airfoils computed by XFOIL [8] using the effective aspect ratio AR_{eff}.

By combining Eq. (5) with Eq. (1) and (2), and solving these equations iteratively, the flow field and force data can be obtained for the whole rotor.

2.2 Aeroacoustic analysis

2.2.1 Broadband noise

In this section, Amiet's method is used to compute the turbulent boundary layer - trailing edge (TBL-TE) noise [5]. The far-field acoustic power spectral density (PSD) S_{pp} for an observer located in the mid-span plane at position $(x, y = 0, z)$ for a given angular frequency (ω) can be written as

$$S_{pp}(\omega) = \left(\frac{\omega b z}{2\pi c_0 \sigma^2}\right)^2 l_y(\omega) d |\mathcal{L}|^2 \Phi_{pp}(\omega), \tag{6}$$

where b is the semi-chord ($b = c/2$), c_0 is the speed of sound, d is the semi-span, the orientation of the blade is defined by the Cartesian coordinate system as x (chordwise), y (spanwise), and z (normal), $\sigma^2 = x^2 + \beta^2 z^2$, $\beta^2 = 1 - M_a^2$, M_a is the Mach number ($M_a = v/c_0$), $|\mathcal{L}|$ is the norm of the transfer function of the airfoil at (x, y, z) location and $\Phi_{pp}(\omega)$ is the surface pressure spectrum near the trailing edge. As suggested by Amiet [5], the convection velocity U_c was assumed to be $U_c = 0.8v$, and the spanwise correlation length $l_y(\omega)$ is computed as $l_y(\omega) \approx 2.1 U_c/\omega$.

The surface pressure spectrum is calculated by six different semi-empirical wall pressure spectrum (WPS) models, namely Goody [12] in 2004, Rozenberg [13] in 2012, Kamruzzaman [14] in 2015, Hu [15] in 2016, Catlett [16] in 2016 and Lee [17] in 2018. All the boundary layer parameters required by those WPS models were extracted at 99% of the chord by the viscous panel XFOIL code [8]. The semi-empirical WPS models typically lack validation cases at low Re flows, because they were often calibrated based on the empirical database at middle to high Re flows. As a result, to test the performance of these WPS models at low Re flows, they are pre-classified into two groups in this paper based on the boundary layer momentum thickness based Reynolds number Re_θ, which are low Re models (Rozenberg, Lee, Kamruzzaman, $Re_\theta \leq 1000$) and high Re models (Goody, Hu, Catlett, $Re_\theta > 1000$), respectively. Finally, the far-field broadband noise can be expressed as

$$SPL(f) = 10 \log_{10} \left[\frac{2\pi S_{pp}(\omega) \Delta f}{P_{ref}^2}\right], \tag{7}$$

where $P_{ref} = 2 \times 10^{-5}$ Pa and Δf is the spectral resolution.

2.2.2 Tonal noise

In this study, the far-field tonal noise is predicted by the Ffowcs Williams-Hawking (FW-H) equation which has been used extensively due to its robustness and practicality. PSU-WOPWOP, an aeroacoustic tool based on the Farassat 1A formulation of the FW-H equations [6], is used to calculate the thickness and loading acoustic sources. The volume term (quadrupole) is ignored, as the Mach number is very low for the small-scale rotors ($M_a < 0.3$). The integral forms of thickness p'_T and loading term p'_L in Farassat 1A formulation are described by [6].

The method is computationally efficient and can calculate the far field noise using the blade geometry and the surface pressure obtained by the aerodynamic models in Sec. 2.1.

3. Validation

In this section, the numerical methods for aerodynamics and aeroacoustics proposed in Sec. 2 are validated against experimental and benchmark cases.

3.1 Aerodynamic validation

A single impeller cooling fan case was selected to validate the aerodynamic solver. It is an 80 mm diameter fan used in a commercial multiple HDD enclosure system with a design speed of 9000 RPM, which is shown in Fig. 2(a). The tip radius is 37.5 mm, and the hub radius is 18.7 mm. This fan operates at a tip Mach number close to 0.1 and maximum chord-based Reynolds number of approximately 6×10^4. The twist and chord distributions were extracted from ten radial sections of the computer aided design (CAD) file, which is shown in Fig. 2(b).

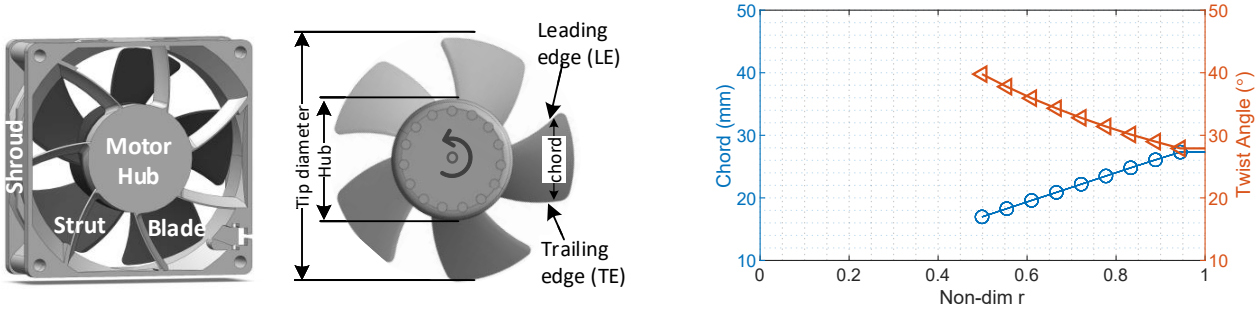

(a) Fan components (b) Twist and chord distributions of fan blades

Figure 2: Geometric characteristics of the selected cooling fan.

The look-up table containing the aerodynamic polar was pre-calculated by XFOIL [8] using the sectional airfoil coordinates extracted from the CAD file. In this study, the aspect ratio correction multiplier M_{AR} selected for this type of fan is 3. The BET-LLT solver was run iteratively to calculate the fan performance curve (P-Q) curve. In order to calculate the 3D blade surface pressure at the required operating condition, the XFOIL [8] code was also integrated into the BET-LLT solver. The 2D airfoil pressure coefficients obtained by XFOIL [8] for each blade section were then assembled into a 3D surface pressure distribution, which can be further used for aeroacoustic calculation.

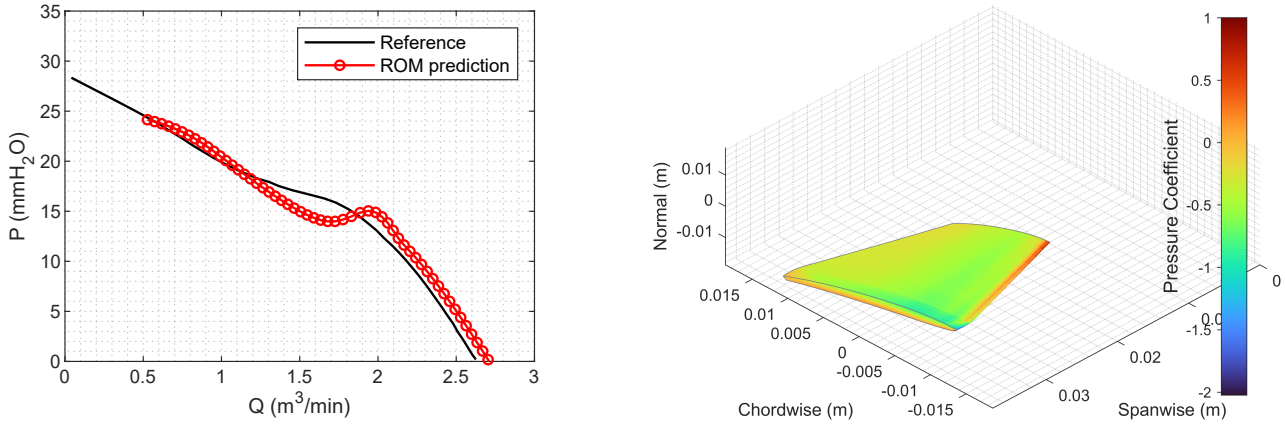

(a) P-Q curve (b) Surface pressure of a fan blade

Figure 3: Aerodynamic validation results.

The aerodynamic validation results are shown in Fig. 3, where (a) shows the predicted fan P-Q curve compared to the reference P-Q curve from the fan manufacturer and (b) shows the predicted pressure coefficient distribution on a single blade at maximum flow rate condition. The predicted results reasonably match with the reference data from the fan manufacturer, which only slightly overpredict the performance at low back pressure conditions, as shown in Fig. 3(a).

3.2 Aeroacoustic validation

A benchmark case was selected to validate the aeroacoustic solver, which is reported in Ref. [4]. The rotor model consists of a two-bladed propeller and the chord-based Reynolds number is from 4.6×10^4 to 10.6×10^4. The structure of this open rotor case is slightly different from the typical cooling fan case shown in Sec. 3.1, but the flow conditions of the sectional airfoils in this open rotor case and cooling fan case are similar since they operate at a resembled Reynolds number flow. To the best of the authors' knowledge, there are no available noise datasets for validating small electronic cooling fans. Hence, this benchmark case with detailed numerical and experimental study in Ref. [4] would be an appropriate case to validate Amiet's model and FW-H method for the noise prediction of the rotating blades.

This rotor was re-designed based on an APC-96 model with the NACA4412 sectional airfoil profile and a 0.15 m tip radius. The CAD file of the rotor geometry was obtained from the first author in Ref. [4]. The test condition selected for validating the numerical method is the 5000 RPM case with a jet exit velocity of 6 m/s, corresponding to the advanced ratio $J = 0.24$. The far-field noise was calculated at a distance of 1.2 m in the rotor plane, corresponding to the microphone location #7 illustrated in Ref. [4]. The benchmark results (i.e., experimental data and high-fidelity simulation data) for this test condition and microphone location were obtained from Ref. [4] for later validations. More details about the experimental and implementations of the high-fidelity lattice-Boltzmann method very large eddy simulation (LBM/VLES) can be found in Ref. [4].

The BEMT model described in Sec. 2 was employed to calculate the flow field of the rotor. The wall pressure spectra were predicted by six different semi-empirical models, where the trailing edge boundary layer parameters were estimated at 99% chord by the XFOIL code [8].

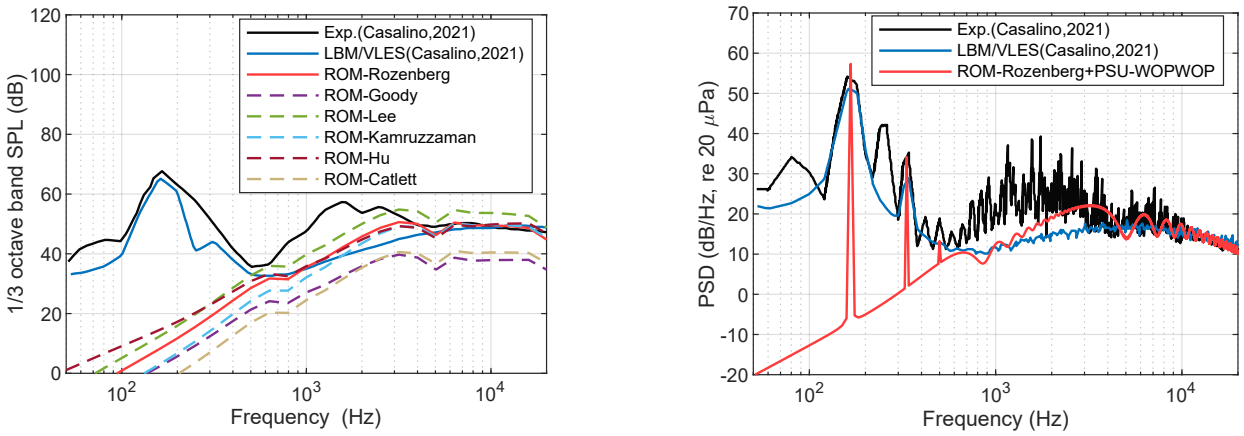

Figure 4: Aeroacoustic validation of ROM against experimental data and high-fidelity LBM/VLES data: (a) broadband noise comparison of sound pressure level (SPL) in third-octave band and (b) total noise comparison of power spectral density (PSD) in narrowband.

The aeroacoustic validation results are presented in Fig. 4, where (a) shows the broadband noise comparison between the aforementioned six WPS models and the benchmark results in the third-octave band, and (b) shows the total noise comparison between the prediction results and the benchmark results in narrowband. Please note that the ROM results in Fig. 4(a) are only broadband noise predictions based on Amiet's model, while the benchmark results consist of both the broadband and tonal noise. As shown in 4(a), all these models provided similar trends but with different noise levels. These models seem to have better performance in the high frequency range (above 3000 Hz), while underestimations can be observed in low frequency range. The low Re models (Rozenberg, Lee, Kamruzzaman) have slightly

better predictions than two of the high Re models (i.e., Goody and Catlett). Overall, it can be argued that the Rozenberg's model shows slightly better performance for broadband noise prediction.

The ROM used Rozenberg's WPS model combined with Amiet's model to calculate the broadband noise and PSU-WOPWOP to obtain the tonal noise. The total noise comparison is shown in Fig. 4(b). It is observed that the ROM's prediction data shows good agreement with the experimental data and the high-fidelity LBM/VLES results. The proposed ROM can accurately predict the first two harmonics of blade passing frequency (BPF) and the broadband noise in the high frequency range. Indeed, it seems in Fig. 4(a) that the humps in the frequency range below 3000 Hz are not predicted. However, the underpredictions correspond to the pure tones in the third-octave band, as can be seen in Fig. 4(b). In addition, the electric motor noise inevitably contaminated noise levels in the frequency range below 3000 Hz, as reported in Ref. [4]. The background noise is also expected to play an important role in frequencies below 200 Hz, since the cut-off frequency of the semi-anechoic chamber is around 200 Hz [4].

This ROM code is written based on the MATLAB platform. The total execution time for this case is about 10 mins on an Intel Xeon E5-2660v3 CPU at 2.2 GHz using 8 cores (1.3 core-hours), which is under 1% of the calculation time of the high-fidelity method (162,540 core-hours) reported in Ref. [4].

4. Conclusion

In this study, a ROM was proposed to efficiently analyze the aerodynamic and aeroacoustic performance of low Reynolds number rotors typically found in the electronics cooling fans. The aerodynamic analysis was achieved using numerical methods based on the BET, while the far-field acoustic analogy was modeled by the Amiet's method for broadband noise and the FW-H equations for tonal noise. The numerical methods were validated against experimental cases at low Re flows. It was shown that the proposed ROM can predict the fan performance curve with fairly reasonable accuracy. In addition, by accounting for the TBL-TE noise, loading and thickness source, the acoustic analogy used in this ROM was found to provide reasonable estimations for both the broadband noise level and tonal BPF harmonics. However, certain discrepancies were observed at BPF harmonics and the broadband noise level, although comparing noise level with experimental data cannot be done extensively due to additional noise sources in the experiments (e.g., background noise, electric motor noise). Overall, the proposed ROM would be highly appropriate for predicting fan performance with reasonable accuracy and low computational cost.

Future experimental testing is planned to validate the proposed numerical methods using different fan geometries. Further investigations of unsteady noise sources from rotor-strut interactions and non-uniform inflow distortions at low Re flows will also be conducted.

5. Acknowledgement

The authors would like to thank Prof. Kenneth Brentner for providing the PSU-WOPWOP software, and Prof. Damiano Casalino for sharing the CAD model of the benchmark case. This work is funded by the China Scholarship Council (202006090041), and the NSF I/UCRC Cooling Technologies Research Center (CTRC) at Purdue University under project 'Thermal Management and Aeroacoustics of Air-Cooled Electronics Enclosures' (2021-2022).

REFERENCES

1. Wasala, S., Xue, Y., Wiegandt, T., Stevens, L. and Persoons, T. Aeroacoustic noise prediction from a contra-rotating cooling fan used in data center cooling systems, *AIAA AVIATION 2021 FORUM*, AIAA Paper 2021-2313, (2021).

2. Garimella, S. V., Persoons, T., Weibel, J. A. and Gektin, V. Electronics thermal management in information and communications technologies: challenges and future directions, *IEEE Transactions on Components, Packaging and Manufacturing Technology*, **7** (8), 1191–1205, (2017).

3. Winslow, J., Otsuka, H., Govindarajan, B. and Chopra, I. Basic understanding of airfoil characteristics at low Reynolds numbers (10^4–10^5), *Journal of Aircraft*, **55** (3), 1050–1061, (2018).

4. Casalino, D., Grande, E., Romani, G., Ragni, D. and Avallone, F. Definition of a benchmark for low Reynolds number propeller aeroacoustics, *Aerospace Science and Technology*, **113**, 106707, (2021).

5. Amiet, R. Noise due to turbulent flow past a trailing edge, *Journal of Sound and Vibration*, **47** (3), 387–393, (1976).

6. Farassat, F. Linear acoustic formulas for calculation of rotating blade noise, *AIAA Journal*, **19** (9), 1122–1130, (1981).

7. Leishman, J. G., *Principles of helicopter aerodynamics*, Cambridge University Press, 2nd edn. (2016).

8. Drela, M. XFOIL: An analysis and design system for low Reynolds number airfoils, *In: Mueller T.J. (eds) Low Reynolds Number Aerodynamics*, **54** (54), 1–12, (1989).

9. Viterna, L. A., Corrigan, R. D. Fixed pitch rotor performance of large horizontal axis wind turbines, *NASA Lewis Research Center: Energy Production and Conversion Workshop*, NASA Lewis Research Center Cleveland, OH, United States, (1982).

10. Allsop, S., Peyrard, C., Thies, P. R., Boulougouris, E. and Harrison, G. P. Hydrodynamic analysis of a ducted, open centre tidal stream turbine using blade element momentum theory, *Ocean Engineering*, **141** (6), 531–542, (2017).

11. Prandtl, L. Report No. 116, Applications of modern hydrodynamics to aeronautics, *Journal of the Franklin Institute*, **193** (3), 431, (1922).

12. Goody, M. Empirical spectral model of surface pressure fluctuations, *AIAA Journal*, **42** (9), 1788–1794, (2004).

13. Rozenberg, Y., Robert, G. and Moreau, S. Wall-pressure spectral model including the adverse pressure gradient effects, *AIAA Journal*, **50** (10), 2168–2179, (2012).

14. Kamruzzaman, M., Bekiropoulos, D., Lutz, T., Würz, W. and Krämer, E. A semi-empirical surface pressure spectrum model for airfoil trailing-edge noise prediction, *International Journal of Aeroacoustics*, **14** (5-6), 833–882, (2015).

15. Hu, N. and Herr, M. Characteristics of wall pressure fluctuations for a flat plate turbulent boundary layer with pressure gradients, *22nd AIAA/CEAS Aeroacoustics Conference*, AIAA Paper 2016-2749, (2016).

16. Catlett, R. M., Anderson, J. M., Forest, J. B. and Stewart, D. O. Empirical modeling of pressure spectra in adverse pressure gradient turbulent boundary layers, *AIAA Journal*, **54** (2), 569–587, (2016).

17. Lee, S. Empirical wall-pressure spectral modeling for zero and adverse pressure gradient flows, *AIAA Journal*, **56** (5), 1818–1829, (2018).